Nickel coatings by Inductively Coupled Impulse Sputtering (ICIS)

LOCH, Daniel A.L. <http://orcid.org/0000-0003-3252-0142>, GONZALVO, Yolanda A. and EHIASARIAN, Arutiun P. <http://orcid.org/0000-0001-6080-3946>

Nickel Coatings by Inductively Coupled Impulse Sputtering (ICIS) technique

Daniel A. L. Loch[(a)], Yolanda A. Gonzalvo[(b)], Arutiun P. Ehiasarian[(a)]

(a) HIPIMS Technology Centre, Materials and Engineering Research Institute,
Sheffield Hallam University, Howard St., Sheffield, S1 1WB, UK
(b) HIDEN Analytical Ltd, Europa Boulevard, Warrington, WA5 7UN, UK
Corresponding author: Daniel A. L. Loch, Email: d.loch@shu.ac.uk

Abstract

Inductively Coupled Impulse Sputtering (ICIS) removes the need for a magnetron, while delivering equal or higher ion-to-neutral ratios compared to other ionised PVD technologies such as High Power Impulse Magnetron Sputtering (HIPIMS). This is especially advantageous for the sputtering of magnetic materials, as these would shunt the magnetic field of the magnetron, thus reducing the efficiency of the sputtering and ionisation process. ICIS produces highly ionised metal-dominated plasma inside a high power pulsed RF - coil with a magnet free high voltage pulsed DC powered cathode.

ICIS operation with magnetic target materials has not been attempted so far. The paper aims to clarify the effects of power and pressure on the chemistry of the deposition flux and is the first investigation of the microstructure of ICIS deposited coatings.

Modelling based on the intensity of the optical emission spectra (OES) is conducted for the first time on the excited species of Ni and Ar in relation to the applied RF-power. Sputtered species show a linear intensity increase for increasing peak RF-power and constant process gas pressure.
The influence of increasing process gas pressure on the ionisation was studied at a constant peak RF-power for pressures. For pressures below 8 Pa the intensity rises, but then remains constant for pressures up to 26 Pa.
The microstructure of Ni coatings shows columnar dendritic or globular growth depending on the ionisation degree. In relation to the film thickness on the top of the substrate, the bottom coverage of unbiased vias with an aspect ratio of 4:1 was 15% and for lower aspect ratios of 1.5:1 was 47.5%.

The current work has shown that the concept of combining a pulsed RF driven coil with a magnet-free pulsed DC powered cathode works well for the sputtering of magnetic material in a stable plasma.

Keywords: ICIS, pulsed plasma source, Ionised PVD, Magnet-free sputtering, deposition on high aspect ratio vias, magnetic material.

1 Introduction

Deposition of thin films of magnetic material is of great importance for various applications such as data recording [1] and magnetic microelectromechanical systems and sensors (MagMEMS) [2-3].

A high degree of ionisation of sputtered species is preferable, as this allows deposition on structured surfaces because ions follow the electric field lines that are created by the potential difference between the plasma bulk and substrate surface and are oriented normally to surface features [4]. This makes it possible to deposit even coatings on sidewalls and the bottom of high aspect ratio features of the substrate [4]. Further this can reduce lattice defect density in the coating and prohibit the early covering of via and trench openings on the substrate, especially on high aspect ratio structures [5, 6].

Magnetron-based sputtering techniques suffer from low target utilisation rates of approx. 40% [7] and low utilisation intervals for magnetic materials as targets need to be thin to allow for sufficient magnetic field strength to be established above the target surface by the magnets of the magnetron [8]. Inductively Coupled Impulse Sputtering (ICIS) is a new development which aims to solve the previously mentioned issues by eliminating the need for a magnetron. ICIS is based on an experimental development by Yukimura and Ehiasarian [9], which utilises high pulsed RF-power in the coil and high pulsed DC voltage on the target to generate dense plasma and attract argon ions (Ar^{1+}) to initiate sputtering. In previous work the RF - plasma assisted high power pulsed glow discharge was adapted to work inside a deposition system and uses a 13.56 MHz RF-power supply to create the basis for a practical application of ICIS technology [10].

In the current work the plasma composition and ionisation mechanisms are studied in detail for the first time. Optical Emission Spectroscopy (OES) was used to analyse Ar^0, Ni^0 and Ni^{1+} ion emission. Further measurements by energy - resolved mass spectroscopy were conducted for Ar^{1+} and Ni^{1+} ion fluxes.

A model based on the optical emission of argon in DC and RF magnetron discharges is used to explain the connection between the intensity ($I(\lambda_{ij})$) and power (P) for magnetron plasma processes. Dony et.al. [11] explain the dependence of the optical emission of the plasma to the power on the cathode. As with ICIS the plasma is generated by an induction coil and not on the target surface, in this study we

correlate the optical emission of the plasma to the power applied to the coil. As the model is based on processes occurring in magnetron plasmas, we compare the ionisation efficiency of ICIS with conventional magnetron processes.

We report for the first time the microstructure of films formed under ICIS conditions and look at the correlations between morphology and plasma chemistry.

The coating microstructure and thickness is analysed by Scanning Electron Microscopy (SEM) and the coating chemical composition and contamination by sputtered RF - coil material by Energy - Dispersive X-ray spectroscopy (EDX).

2 Experimental Details

The experimental ICIS system (shown schematically in Fig.1 and dimensions in Table 1) is set up inside a UHV chamber (Kurt J. Lesker CMS - 18) and consists of a 2-turn 80 mm diameter solid rod copper coil and a magnet-free 75 mm diameter cathode furnished with a high purity (3N) Ni target, a Hüttinger PFG 5000 RF power supply (13.56 MHz) to power an RF - coil and a Hüttinger HIPIMS power supply HMP 6/16 to apply a pulsed DC voltage to the cathode. Argon with a purity of 99.998% was used as process gas.

Table 1 Dimensions of the ICIS setup

Diameter of copper coil:	**7 mm**
Length of copper coil:	500 mm
RF coil (centre) to substrate distance:	127 mm
Target to substrate distance:	130 mm

Due to the highly ionised metal plasma that is produced by ICIS, we do not expect to see an influence on the morphology of the coating by the tilt angle between the target and substrate normals. Ionised species would follow the electrical field lines perpendicular to the substrate surface. Additionally, the operating pressures are sufficiently high that we could expect a high number of collisions of metal with the working gas resulting in a randomised (as opposed to directional) flux of depositing particles to the surface of the substrate. However, due to the remaining neutral species in the flux some influence on the top corner of the via can be expected.

The plasma discharge is created within the area of the induction coil driven with pulsed RF power. When the RF plasma has ignited, pulsed DC power is applied to the cathode to attract positive Ar ions to the target surface to initiate sputtering. RF and DC power pulses are synchronised by a pulse generator.

In the current study a pressure vs. RF - power matrix was used to examine the influence on the ionisation in the discharge and deposition flux properties. The pulsed DC voltage was kept constant at 1900 V. The working pressure was varied from 2.96 to 21.4 Pa by increasing Ar flow. Peak RF - power was varied between 1000 - 4800 W applied at a repetition frequency of 500 Hz with a pulse width of 150 µs. These settings result in a duty cycle of 7.5%, reducing the average power and thermal load on the coil. The base pressure was in the region of $5x10^{-5}$ Pa.

Thin film deposition was carried out on silicon dioxide (SiO_2) substrates with vias that were held at floating bias potential. In this series of experiments, the aspect ratio (AR) is the relation of depth to width of the via. Temperature on the substrate at the beginning of the process was between 20 - 28 ºC and no further substrate heating was applied. During deposition the temperature rose by 6 - 8 ºC/hour. The deposition rate was approx. 125 nm/h (0.35 Å/s) at a RF power setting of 4000 W and a pressure of 6.4 Pa and approx. 50 nm/h (0.14 Å/s) for a pressure of 14 Pa.

2.1 Plasma and Coating Characterisation Techniques

Plasma composition analysis was carried out by OES monochromator (Jobin Yvon Triax 320, HORIBA Synapse CCD detector) with *in vacuo* quartz optical fibre and collimator placed as indicated in Fig. 1. The spectra resolution is 0.12 nm (1200 grooves/mm in the grating), the focal length of the monochromator was 320 mm and the entrance slit size 0.06 mm.

The fibre is connected to a collimator lens which is protected by a sapphire window inside a 90 mm long, 8 mm internal diameter lens cover that protects the optical fibre from being coated. The spatial resolution is 10 mm, acceptance angle is nominally 2.5 degrees.

The comparison of the excitation efficiency of ICIS with conventional ICP magnetron sputtering is done by using the OES measurement results for increasing RF - Power in the model for ionisation by

electron and Penning collisions developed for RF - coil enhanced magnetron sputtering described in section 2.2.

Energy resolved mass spectrometer (Hiden Analytical PSM 003) was used to measure the ion content and ion energy for Ar^{1+} and Ni^{1+} in the ICIS plasma at a position near the substrate as shown in Fig.1. The energy spectra resolution of the instrument is below 0.5 eV.

SEM (FEI NovaSEM 200) was used to examine the coating properties and to determine the structure and bottom coverage (BC). The bottom-coverage, is a value for the percentage of cover on the bottom of a via compared to the film thickness on the surface of the substrate. An EDX system (Oxford Instruments X-Max detector and INCA analysis software) and 20 keV electron beam were used to obtain the relative composition of the films.

Magnetic properties of the films were measured by Magneto Optical Kerr Effect Spectroscopy (MOKE) at the University of Lisbon. MOKE hysteresis loops were obtained from measurements of the polarization angle of a He - Ne laser (wavelength 633 nm, power 0.5 mW and 1 mm beam diameter) in longitudinal geometry where the magnetic field to the sample was applied in the film plane.

2.2 Modelling of the Excitation Properties

As with ICIS a magnetron is not used to trap the electrons close to the target surface, it is of interest to see how the ICIS process compares to magnetron based sputter processes in terms of excitation and ionisation efficiency of the process gas and sputtered material. Dony et al.[11] have looked at the ionization in RF driven magnetron processes and optical emissions thereof. In the following we will explain how the Dony model is used to explain the ionisation behaviour of ICIS plasma.

Emission intensity measurement results in section 3.2 showed an increase in gas and metal excitation and ionisation as a function of power. Generally, the relation between emission intensity of the element (I_{El}) and RF - power (P) in the coil is expressed by a power law with an exponent that is specific to each species.

For the intensity of argon neutrals and metastables we experimentally obtain the following relation: $\log(I_{Ar}) = \beta \log P$ (1), where I_{Ar} is the intensity of Ar for a chosen wavelength, P is the power applied to the RF coil and β is the slope obtained for Ar^0.

As the excitation of Ar is predominantly by electron collision the emission intensity $I_{Ar} = K_{Ar} \cdot n_{Ar} \cdot n_e \cdot C^{Ar}$ (2) can be assumed as proportional to the electron density n_e, from this follows: $I_{Ar} \propto n_e$ (3).

From equation (1) and (3) it can be concluded that $n_e \propto P^{\beta}$ (4).

For the excitation of metal neutrals the intensity is $I_{Me} = K_{Me} \cdot n_{Me} \cdot n_e \cdot C^{Me}$(5). Where K_{Me} is a function of the spectral response of the spectrometer and the radiative frequency and can be considered constant for a given line, n_{Me} is the metal atom density and n_e is the electron density. C^{Me} is the production rate by electron collisions and depends on electron temperature, which we assume to be constant for constant pressure and increasing applied power. To assess the temperature shifts as a function of power we analysed the emission line ratio of Ni neutral excitation at different energy levels 310.54 nm (34408 cm^{-1}) and 373.68 nm (57789 cm^{-1}) as compared to 373.92 nm (28086 cm^{-1}). These ratios are sensitive to changes in electron temperature similar to the differences in energy levels. The results (not shown) indicated changes in ratio for the lower temperatures which increased for powers up to 3000 W and were constant thereafter. The ratio was constant for the higher temperatures. This indicates that the fluctuations in temperature were small and can be neglected. This could be attributed to the high operating pressures of the process which induce a high frequency of collisions during which electrons are thermalised efficiently.

The definition of the sputtering yield is $n_{Me} = \varepsilon \gamma_e (n_{Ar^+} + n_{Me^+})$ (6), where ε is a constant and γ_e is the weighted sputtering coefficient for gas and metal sputtering. As plasma can be considered to be quasineutral, the Ar and metal ion density is equivalent to the electron density $(n_{Ar^+} + n_{Me^+}) \approx n_e$(7). By substituting $(n_{Ar^+} + n_{Me^+})$ with n_e in equation (6) and inserting in equation (5) it can be concluded that $I_{Me} \propto {n_e}^2$ (8). Following from equations (4) and (8) for metal neutrals we can conclude that $I_{Me} \sim \left(P^{\beta}\right)^2$ (9). From this follows that for Ni neutrals in a logarithmic scale the slope β is twice as steep as for Ar neutrals: $\log(I_{Ni^0}) \sim 2\beta \log P$ (10). Assuming electron collisions to be the

main ionisation mechanism we can assume the metal ion density ($n_{Me^{1+}}$) to be

$n_{Me^{1+}} \sim n_{Me} \cdot n_e$ (11). Further from equations (4), (6) and (7) we know that $n_{Me} \sim {n_e}^2$(12).

Combining eq (4), (11) and (12), we obtain: $\log(I_{Ni^{1+}}) \sim 3\beta\, logP$ (13) for Ni ions. The coefficient of proportionality is higher because a further electron collision is necessary to ionise the metal atoms. This means that the slope of Ni ions is expected to be three times steeper than that of excited Ar neutrals. This is consistent with the findings for conventional DC magnetron sputtering by Rossnagel and Saenger [12].

Furthermore, Penning ionisation of the metal vapour by collisions with Ar metastables (Ar^*) needs to be taken into account due to the high operating pressures of the discharge which increase the collision cross section for these types of collisions to be similar that of electron collision processes. In analogy to the electron collision process, in Penning ionisation the densities of sputtered metal are proportional to the density of electrons; $n_{Me} \approx n_e$(14), see eq. (6) and (7). The ionisation of neutral species is facilitated by collisions with metastable Ar*, this means that $n_{Me^{1+}} \propto n_{Me} \cdot n_{Ar^*}$ (15). This is in turn proportional to $n_{Me} \cdot n_{Ar^*} \propto n_{Me} \cdot n_e$ (16). Using eq. (14) we can substitute n_{Me} with n_e and obtain $n_{Me^{1+}} \propto {n_e}^2$ (17). The emission intensity can be seen to be related to the density of ions and electrons, as a further collision is necessary to excite the ion; $I_{Ion} \propto n_{Ion} \cdot n_e$ (18). With equation (17) it can be seen that the metal ion intensity is $I_{Me^{1+}} \propto {n_e}^3$ (19). This analysis indicates that both electron collision and Penning ionisation lead to a similar trend for intensity vs. plasma density and applied RF power.

3 Results & Discussion

3.1 Plasma Emission Results

Optical spectra for an ICIS 3000 W Ni plasma in Fig.2 show strong emission from Ni neutrals. Ni ions were found on the only strong emission line in the visible spectrum at a wavelength of 333.188 nm. This line is a convolution of the 333.103 nm and 333.287 nm lines which have similar weighted oscillator strengths of 0.163 and 0.138 respectively, calculated with values from Ochsenbein et.al. [13]. Most Ni ions can be expected to emit at lower wavelengths very much further in the ultraviolet

spectrum. Additional experiments were conducted by mass- and energy- resolved spectroscopy to detect these, as discussed separately in section 3.3.

3.2 Influence of Applied RF - Power on Ionisation and Modelling

Fig. 3 shows measured OES intensities against RF-coil power in a log-log graph for the ICIS of Ni plasma. From the slope of excited Ar we obtain an exponent $\beta = 0.34$, which is approx. half the value for the Ar emission from the 4p level for RF-MS [11] and one third of value reported for DC-MS [12]. The slopes for excited Ar and Ni neutrals (Table 2 contains the observed gas and metal species) fit very well to the model with the Ni^0 intensity rising with a factor of 2 faster compared with Ar^0. The only deviation from the model is the saturation of Ni^0 intensity for RF-power settings above 3000 W. For Ni ions the slope of the log intensity is three times the slope of Ar^0 for RF-power settings below 3000W. This is consistent with excitation by electron collisions and ionisation by either electron or Ar* metastable collisions as described by the used model. Several factors could be the cause for the deviation from the model, such as increased ionisation efficiency for powers above 3000 W by Penning ionisation, a reduction of the mean free path and higher electron temperatures.

Table 2 List of observed gas and metal species data and observed and predicted slope values of intensity-power modelling

Species	Wavelength (nm)	Osc. Strength	Slope	
			observed	predicted
Ar^0	750.387	0.339	0.34	-
Ar^0	751.465	0.316	0.33	0.34
Ar^0	763.511	1.047	0.36	0.34
Ni^0	310.188	0.568	0.78	0.68
Ni^0	313.411	0.533	0.87	0.68
Ni^{1+}	333.188	0.163-0.138	1.12	1.02

The ion to neutral ratio in Fig. 4 for increasing RF power at a constant pressure shows a doubling of the ratio from 2000W to 4000W. This means that the influence of ions on the coating will change largely in this regime. Especially for deposition into high AR vias the higher ion to neutral ratio is

known to enable a better coverage and film growth on sidewalls and bottom. For AR larger than 3:1 the deposition on the bottom of the via is mainly by ions, as has been shown by Rossnagel [4]. The higher ratio of ions to neutrals also allows for denser coatings with metal ions being more efficient than gas [14].

3.3 Influence of Process Pressure on Ionisation

Figure 5 describes the influence of pressure on the ionisation at a constant power of 3000W. For pressures below 10 Pa there is a linear intensity increase for all gas and metal species. For pressures of 10-20 Pa, the Ar neutral intensity remains constant, while the Ni neutral intensity decreases between 10 Pa and 15 Pa; remaining constant for pressures up to 26 Pa. Ni ion intensity remains constant for all pressures above 10 Pa. This is also confirmed by the ion to neutral ratio plot in Fig. 6 where there is no change in the ratio.

This could be due to the constant RF power that is not sufficient to allow further excitation or ionisation of metal species at pressures higher than 10 Pa.

3.4 Mass and Energy Resolved Spectroscopy

The energy of impinging ions on the surface of the substrate is an important factor in densifying the structure of the film [14]. For magnetic materials, where the domain size is approx. 50 nm, to achieve bulk material properties in a thin coating it could be beneficial to promote densification of the coating. Fig. 7 shows the measurement for Ni^{1+} and Ar^{1+} ions at 3000 W and 13 Pa. The energy distribution follows a non-Maxwellian distribution with a narrow ion energy bandwidth. The highest intensity peak energy is 20 eV which corresponds to the plasma potential. This energy has been found to be an ideal level for ion surface mobility without inducing lattice defects. This low energy level and high ion to neutral ratio make it suitable for production of dense coatings [14]. A further lower intensity peak is visible at 170 eV corresponding to high energetic ions which can be found also in pulsed plasmas [15]. To determine the origin of these energetic ions further work is necessary which lies outside the scope of this paper.

3.5 Coating properties

For the examination of the coating properties we deposited Ni for a range of power and pressure values from the matrix used for the plasma study in sections 3.1 and 3.2. From the plasma study it was concluded that a pressure of approx. 14 Pa would be sufficiently high to study the influence of power on the coating, as the influence of pressure on the plasma does not change significantly above 10 Pa. Power settings of 2000W, 3000W and 4000W applied peak RF-power were chosen to evaluate the influence of power.

Fig. 8a shows the cross section of the coating deposited at 2000W RF-power in a via with AR 3:1. A dense globular microstructure can be observed near the surface. A good bottom and sidewall coverage are visible

The accumulation of material at the bottom of the structure indicates deposition by ions [16]. The overall distribution of the deposit indicates that the majority of the deposited species were metal ions. The dense structure of the bottom coating and no visible separation between the sidewall and bottom as well as the even sidewall coverage suggest only modest resputtering from the bottom of the via.

Figures 8b (3000 W RF-power) and 8c (4000 W RF-power) exhibit the same features of the coating on the substrate surface as well as the sidewalls and bottom of the via. However, as can be seen from the insets, the microstructure changes with increasing applied RF-power. The grain size reduces and grain boundaries are obscured resulting in a denser coating microstructure. This is consistent with an increased ionisation rate of the deposition flux (Figure 4) which provides adatoms with high energy and long diffusion paths on the surface of the growing film.

The influence of pressure on the coating morphology at a constant power setting of 4000W RF power can be seen when comparing Fig. 8c and Fig. 8d. Fig. 8d shows a cross sectional SEM image of a via with an AR of 2:1 at low pressure (6.4 Pa). These conditions result in a medium ionisation degree of the sputtered material. The films exhibit dense columnar dendritic growth. Similar results for the microstructure have been shown by Linnik et.al. [17], albeit these coatings were deposited in a N_2

atmosphere and as such have reduced magnetic properties, compared to pure Ni coatings. For the above mentioned process settings and AR the BC is 21.2 %.

The coating deposited at the higher pressure of 14 Pa exhibits a denser globular structure (Fig. 8c). The factor 2 increase in pressure resulted in a factor of 2.5 reduced deposition rate due to increased elastic scattering of the depositing species by the process gas and reduced diffusion rate. Generally increasing the pressure causes collisional thermalisation of the depositing species, reduction of their energy and mobility on the surface of the growing film resulting typically in a reduced coating density.

Close-up images of the whole length of the via of the samples coated at 4000W applied RF-power with pressure settings of 14.3 Pa (Fig. 9a) and 6.4 Pa (Fig. 9b), clearly show that the growth of columns on the sidewalls is mostly perpendicular to the substrate surface and homogeneously level over the whole length of the sidewall of the feature.

To understand the effect of pressure on morphology we analyse the fluxes of species to the growing film. The gas ion is likely to be unaffected by pressure as they are created mainly by electron impact which is related to the density of plasma and RF power. This is supported by the constant emission of Ar I (Figure 5). At the same time the deposition flux to the substrate is reduced significantly due to scattering. These two effects amount to an elevated gas ion-to-metal neutral ratio with pressure and result in enhanced mobility and densification of the microstructure at higher pressures. This is supported by the significantly better side wall coverage for the 14.3 Pa film visible in Fig. 9a. The open top of the via is consistent with gas-induced resputtering at the corner. The increase in ion-to-neutral ratio also drives a shift in the growth mode of the film on the surface from well-defined columnar to dense globular. In comparison, at the lower ion-to-neutral ratio (Fig. 9b) the growth is typical of Zone 2 of the Thornton structure zone diagram, where columns are enlarged and have dense grain boundaries. The column width is similar at the bottom as well as at the top indicating that the texture selection is complete. Already at the interface the grain size is large indicating that nucleation sites coalesce into larger domains whose subsequent growth is not competitive therefore leading to fast establishment of texture and dense morphology of the film. For the higher pressure of 14.3 Pa, the microstructure seems to be shifting towards the dense Zone T of the Thornton model.

No significant sputtering of the RF coil was observed in these experiments. From Table 3, it can be seen that over process time the contamination by RF-coil material can be reduced to below the detection limit of SEM-EDX. Cu and In contaminants were detected as remnants from other deposition in the chamber. This can be related to an observed net deposition of target material on the coil during the process.

Table 3 Coating composition of a process series showing reduced contamination by RF coil material or other impurities.

Sequence	**1 (0h)**	**2 (4h)**	**3 (8h)**
Power / Pressure	4000W / 14.1 Pa	4000W / 24.7 Pa	3000W / 14.3 Pa
Element	Weight %	Weight %	Weight %
Ni	90.30	94.58	100.00
In	6.34	5.42	-
Cu	3.37	-	-

3.6 Magnetic Properties of the Coating

Magnetic properties of the films were measured by Magneto Optical Kerr Effect Spectroscopy (MOKE). MOKE hysteresis loops were obtained from measurements of the polarization angle of a He - Ne laser (wavelength 633 nm, power 0.5 mW and 1 mm beam diameter) in longitudinal geometry where the magnetic field to the sample was applied in the film plane.

As can be seen in Fig. 10a-c, all samples gave a MOKE typical hysteresis response. Fig.10a shows a slightly different hysteresis curve with a slope in the intensity values above the coercivity values. This sample has the highest Ni purity of the process series shown in section 3.4. Due to these features, this sample was compared to that of a standard 25 nm permalloy (Py) (80 % Ni, 20 % Fe) film on glass substrate. Fig. 11 shows the comparison of the hysteresis loops of Ni and Py with the MOKE intensity of Ni being 1.2 times larger than that of Py and approx. doubled coercivity value of 6 Oe. The MOKE response is the product of reflectivity and Kerr rotation [18]. With the Ni showing a MOKE response of 1.2 times larger than Py and the reflectivity of Py and Ni measured to be 0.5, the Kerr rotation of Ni

is 0.6 times that of Py. The Kerr rotation is proportional to the magnetisation and for Py is well measured to be 10.0 kG, which is close to the calculated literature value of 9.5 kG [19]. For the Ni coating this corresponds to a magnetisation of 6.0 kG, which is close to the typical magnetisation of Ni in bulk form [19].

4 Conclusions

Successful deposition of a magnetic material has been demonstrated by ICIS for the first time while achieving high degrees of metal ionisation. The benefits of this are deposition into high aspect ratio structures with good sidewall and bottom coverage. Further a more uniform thickness coating can be deposited on sidewalls due to the perpendicularly approaching electric field lines and high metal ionisation; columns can grow with horizontal orientation on the vertical sidewalls of vias with high aspect ratios.

Calculations of the excitation and ionisation in ICIS processes have shown to be comparable to magnetron based systems up to 3000 W RF-power for Ni. For higher powers further factors increase the ionisation efficiency of sputtered material. At high pressures the coating density was significantly improved due to an increase in gas ion-to-metal neutral ratio.

Acknowledgements

The authors would like to thank Prof. Olinda Conde and Nikolay Polushkin from the University of Lisbon, Portugal, whose cooperation in the MOKE measurements we greatly appreciate.

References

[1] WHITE, R.M. (1990). The Materials Aspect of Magnetic Recording. *Journal of Magnetism and Magnetic Materials*. **88**, 165 - 176.

[2] GIBBS, M.R.J. et.al. (2004). Magnetic Materials for MEMS applications. *J. Phys. D: Appl. Phys* . **37**, R237 - R244.

[3] NIARCHOS, D (2003). Magnetic MEMS: key issues and some applications. *Sensors and Actuators A,* **109**, 166-173.

[4] ROSSNAGEL, S (2000). Ionisation by Radio Frequency Inductively Coupled Plasma. *Thin Films,* **27**, 37-65.

[5] MÜLLER, K-H (1987). Ion-beam-induced epitaxial vapor-phase growth: A molecular-dynamics study. *Phys. Rev. B,* **35**, 7906-7913

[6] ANDERS, A (2007). Metal plasmas for the fabrication of nanostructures. *J. Phys. D: Appl. Phys.* **40**, 2272-2284

[7] CHAPMAN, B (1980). Glow Discharge Processes: Sputtering and Plasma Etching. *Wiley-Interscience; 1 edition*.

[8] WINDOW, B, SHARPLES F (1985). Magnetron Sputtering Sources for Ferromagnetic Material. *J. Vac. Sci. Technol.* **A 3 (1)**, 10-13.

[9] YUKIMURA, K and EHIASARIAN, A P. (2009). Generation of RF plasma assisted high power pulsed sputtering glow discharge without using a magnetic field. *Nuclear instruments and methods in physics research section B: Beam interactions with materials and atoms,* **267** (8-9), 1701-1704.

[10] LOCH, D A L, EHIASARIAN, A P. (2012). A novel sputtering technique: Inductively Coupled Impulse Sputtering (ICIS). *IOP Conf. Ser.: Mater. Sci. Eng.* **39** 012006

[11] DONY, M.F; RICARD, A.; DAUCHOT, J.P.; HECQ, M.; WAUTELET, M. (1995). Optical diagnostics of d.c. and r.f. argon magnetron discharges. *Surface and Coatings Technology,* **74-75**, 479-484.

[12] ROSSNAGEL, S.M.; SAENGER, K.L. (1989). Optical emission in magnetrons: Nonlinear aspects. *J. Vac. Sci, Technol.,* **A7(3)**, 968-971.

[13] OCHSENBEIN, F; BAUER, P.; MARCOUT, J; (2000). Astron. Astrophys., Suppl. Ser., **143**, 23-32.

[14] PETROV, I; et.al. (2003). Microstructural Evolution during Film Growth. *J. Vac. Sci, Technol.,* **A21**, S.117.

[15] BRADLEY, J, et.al. (2002). The distribution of ion energies at the substrate in an asymmetric bi-polar pulsed DC magnetron discharge. *Plasma Sources Sci. Technol.*, **11**, 165–174.

[16] ROSSNAGEL, S.M.; HOPWOOD, J. (1993). Metal Ion deposition from ionized mangetron sputtering discharge, *J. Vac. Sci, Technol.,* **B12(1)**, 449 - 453.

[17] LINNIK, A.I.; et.al. (2012). Synthesis and Magnetic Properties of Nanocolumnar Nickel Films Deposited in Argon-Nitrogen Athmosphere. *Technical Physics Letters,* **Vol.38**, No.6, 499 - 502.

[18] ALLWOOD, D; et.al. (2003). Magneto-optical Kerr Effect Analysis of Magnetic Nanostructures, *J. Phys. D: Appl. Phys.,* **36**, 2175 - 2182.

[19] TEBBLE, R.S.; CRAIK, D.J. (1969). Magnetic Materials. *Wiley-Interscience; 1. edition.*

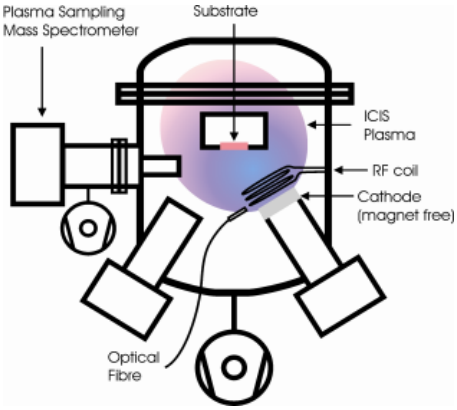

Figure 1 Experimental setup of the ICIS deposition system with the assembly of the inductive coil, magnet-free cathode and OES location. The angle between target and substrate normals' is 32 degrees.

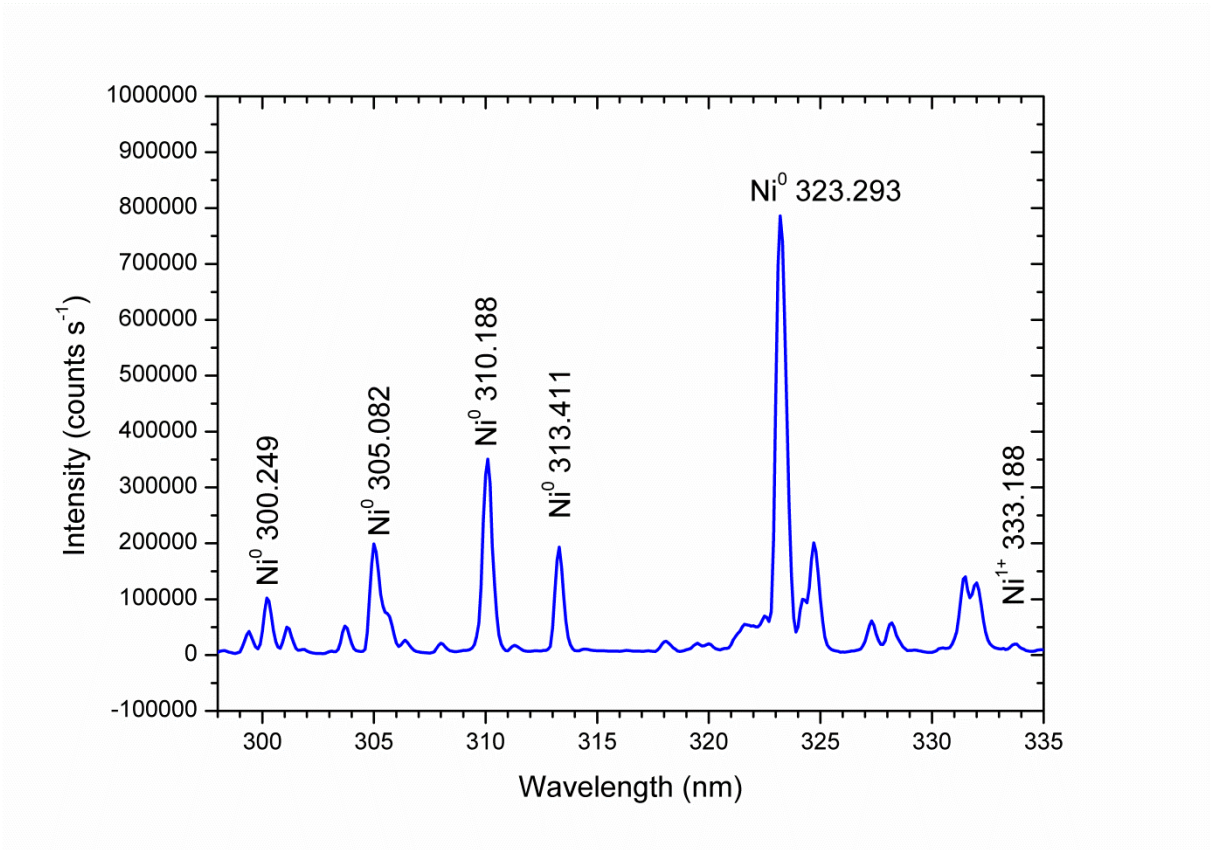

Figure 2 OES Graph of the emission intensity of Nickel in ICIS plasma. Clearly visible are the high intensity Ni neutral lines. Ni ion line is the strongest line in the visible spectrum. Applied RF power was 3000W.

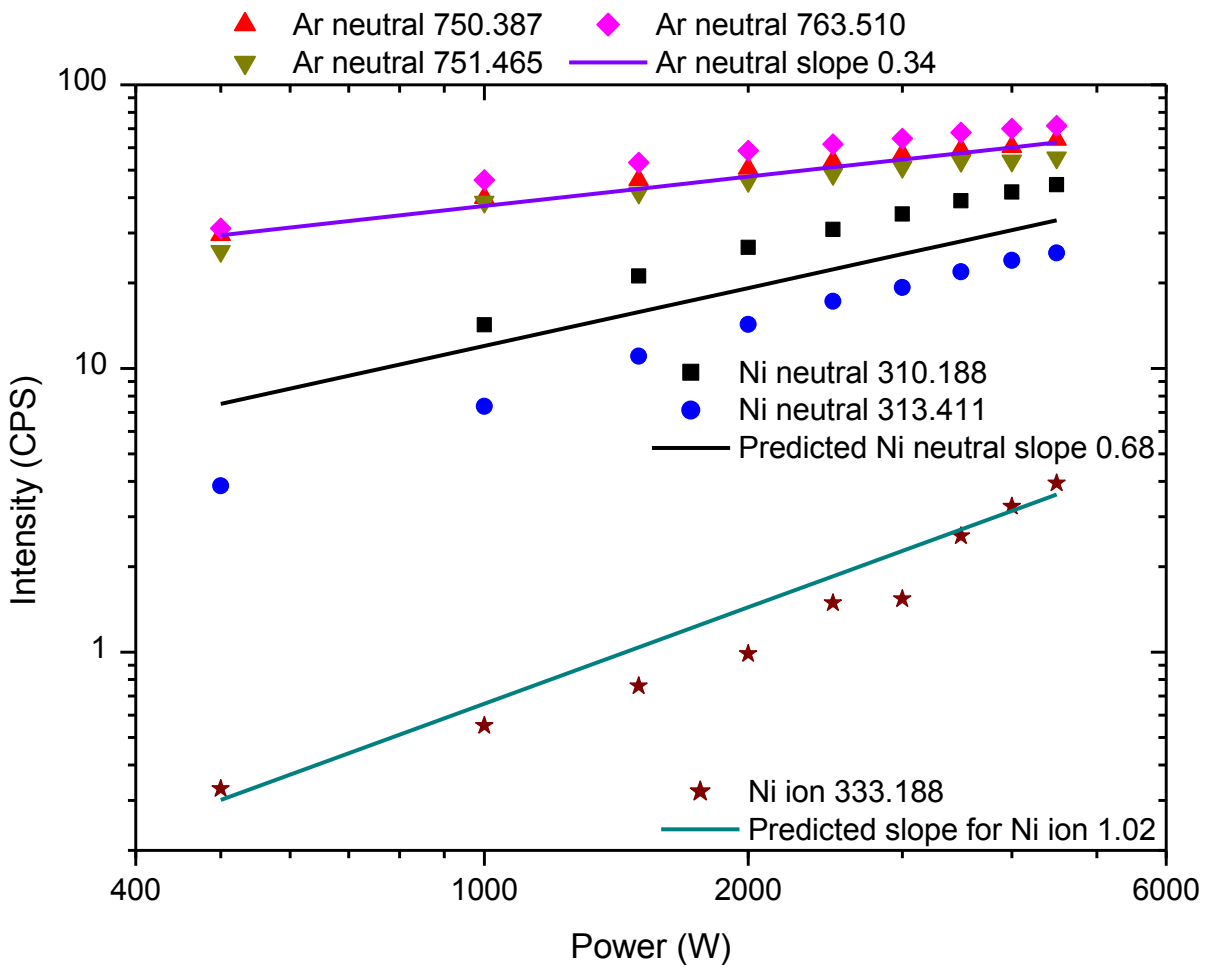

Figure 3 Measured results for Ar and Ni neutrals for a constant pressure of 12 Pa with varying RF-Power.

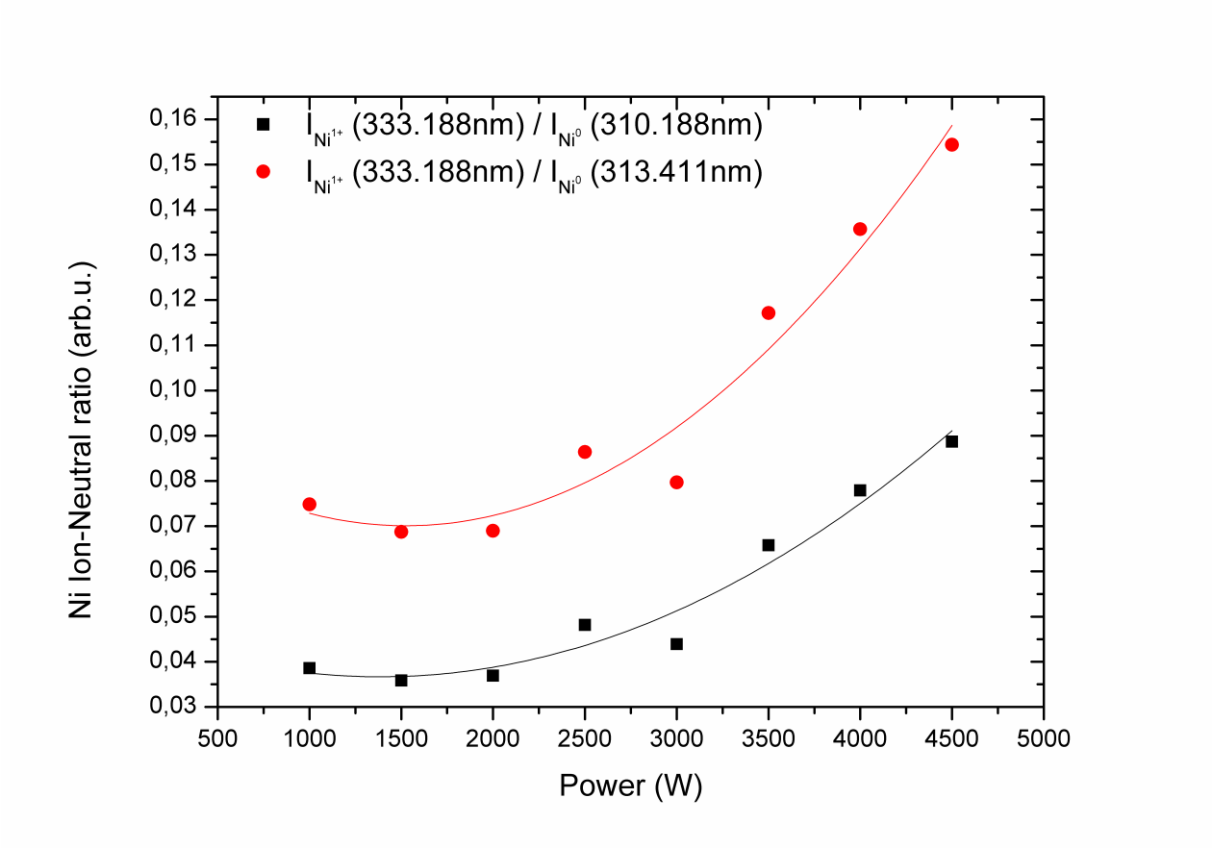

Figure 4 Ion to neutral ratio of ICIS Ni plasma for increasing RF power at constant process pressure. Emission lines used were: Ni^{1+} at 333.188 nm, Ni^{0} at 310.188 nm and Ni^{0} at 313.411nm.

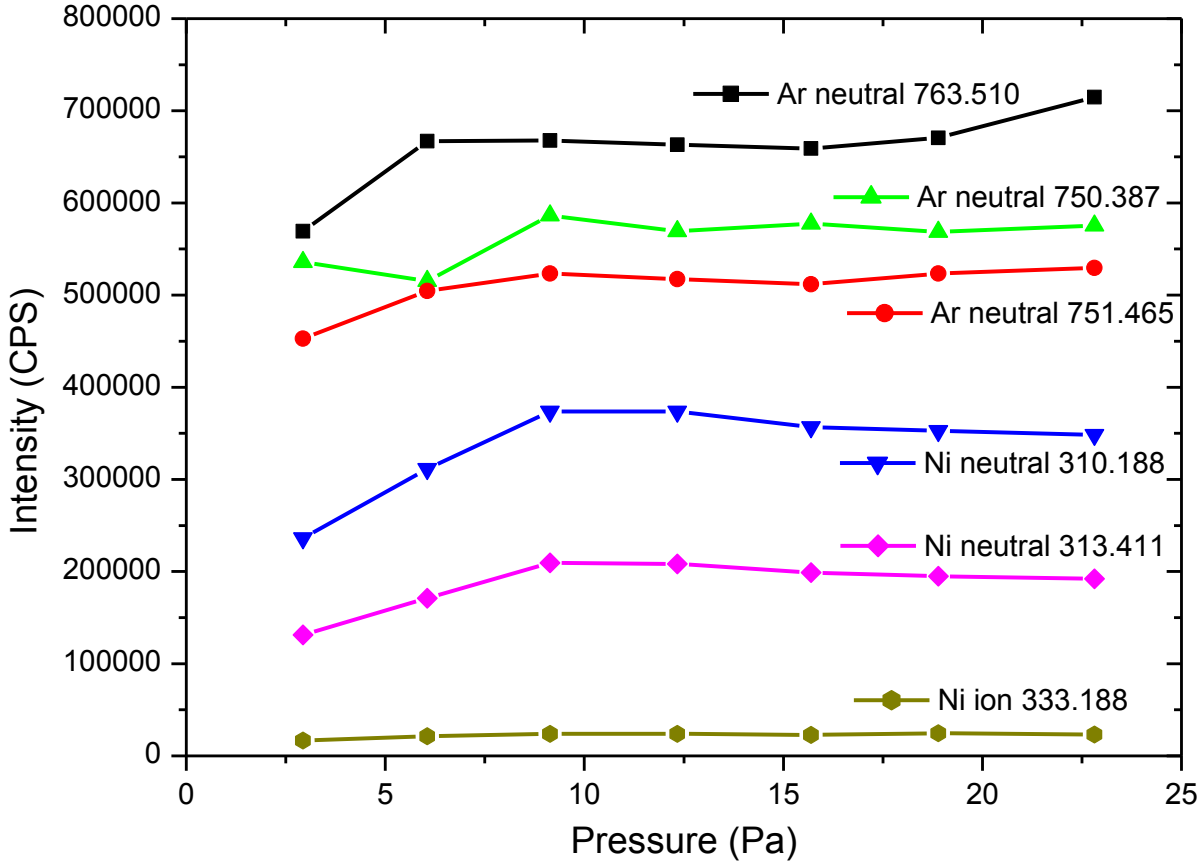

Figure 5 Measured results for Ar and Ni neutrals for a constant RF-Power of 3000 W and varying pressure.

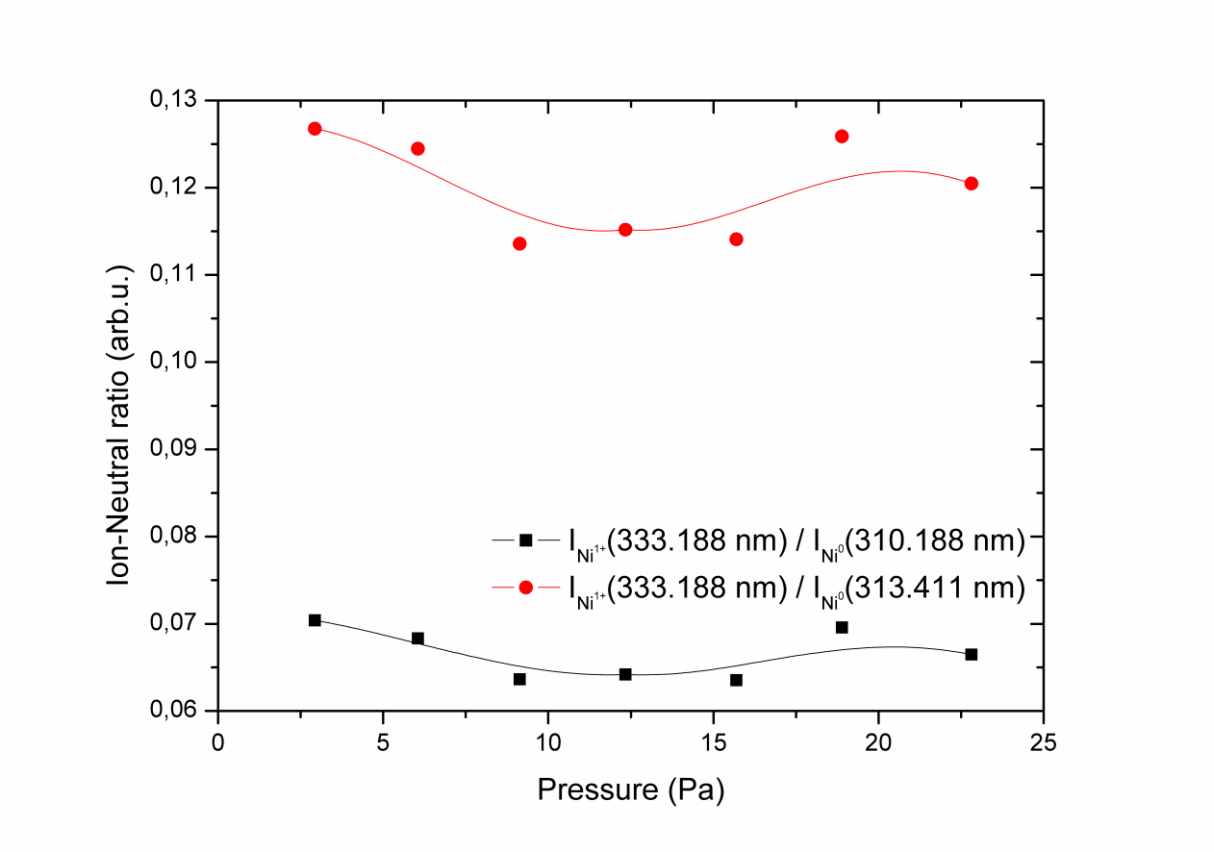

Figure 6 Ion to neutral emission ratio of ICIS Ni plasma for constant power and increasing pressure. Emission lines used were: Ni^{1+} at 333.188 nm, Ni^{0} at 310.188 nm and Ni^{0} at 313.411nm.

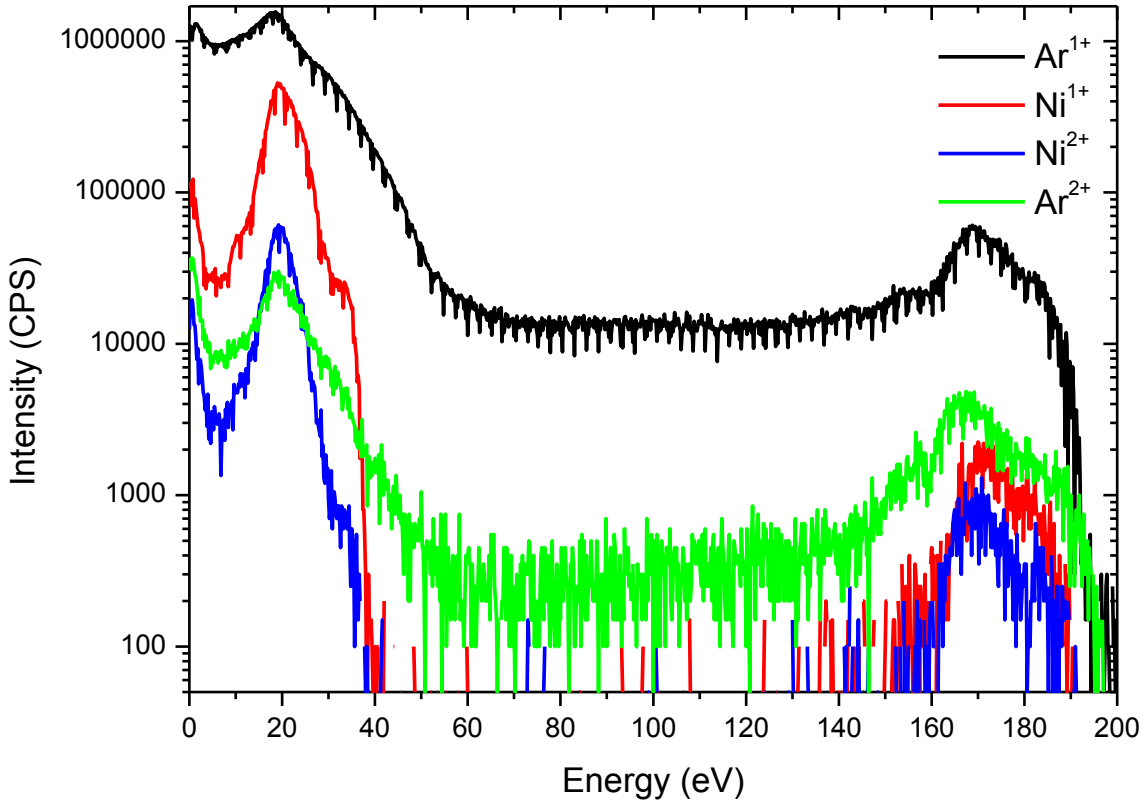

Figure 7 Ni ion energy distribution for a ICIS plasma. 20eV is an ideal energy level for increased surface mobility and reduced lattice defects. A second, lower intensity peak is at 170 eV. The double charge of the ion has not been considered in the energy axis.

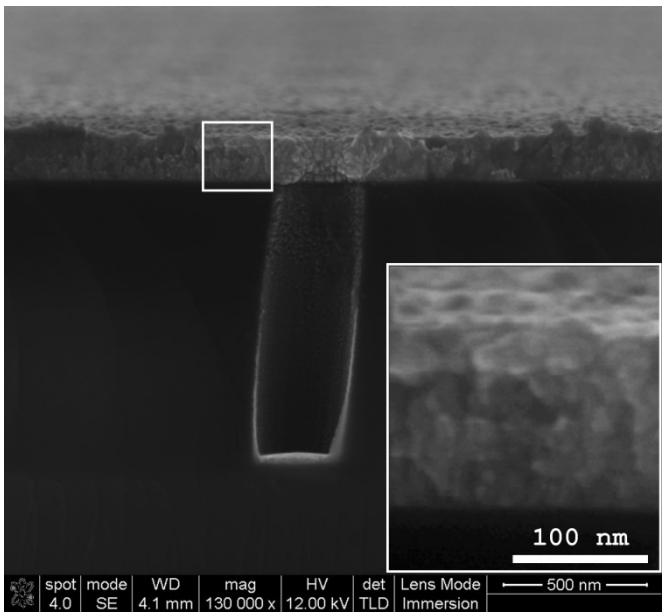

Figure 8a SEM cross section of Ni coated via with an AR of 3:1. Deposition parameters 2000W applied RF-power in ICIS plasma, process pressure 14Pa. The insert shows magnified image of the coating exhibiting dense globular structure. Deposition rate is 40nm/h.

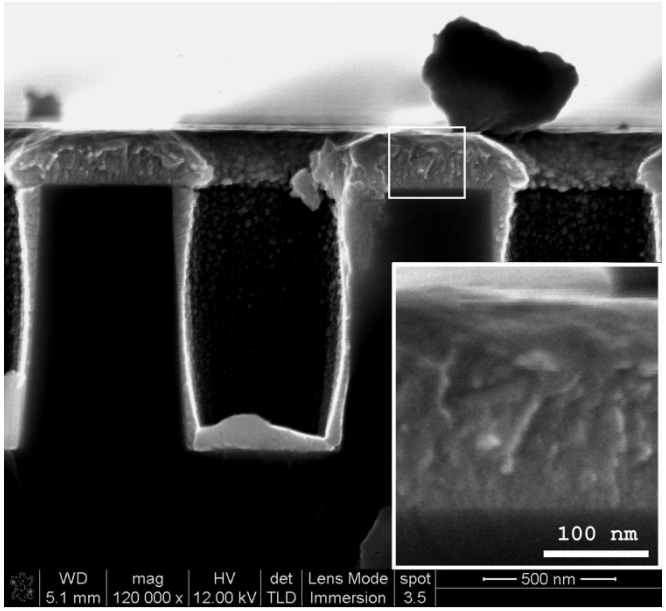

Figure 8b SEM cross section of Ni coated via with an AR of 2:1. Deposition parameters 3000W applied RF-power in ICIS plasma, process pressure 14Pa. The insert shows the magnified image of the coating showing dense globular structure, but with a smaller feature size than with 2000W applied RF-power. Deposition rate is 50nm/h.

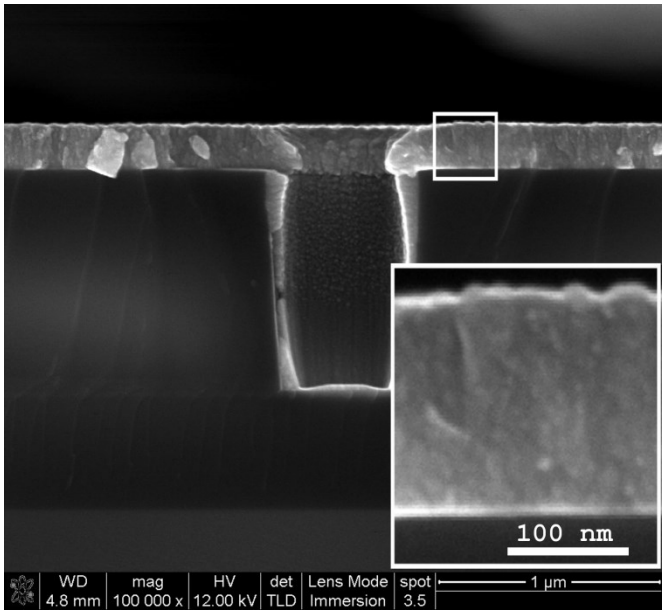

Figure 8c SEM cross section of Ni coated via with an AR of 2:1. Deposition parameters 4000W, applied RF-power in ICIS plasma, process pressure 14Pa. The insert shows the magnified image of the coating showing dense globular structure, but with a smaller feature size than with 3000W applied RF-power. Deposition rate is 45nm/h.

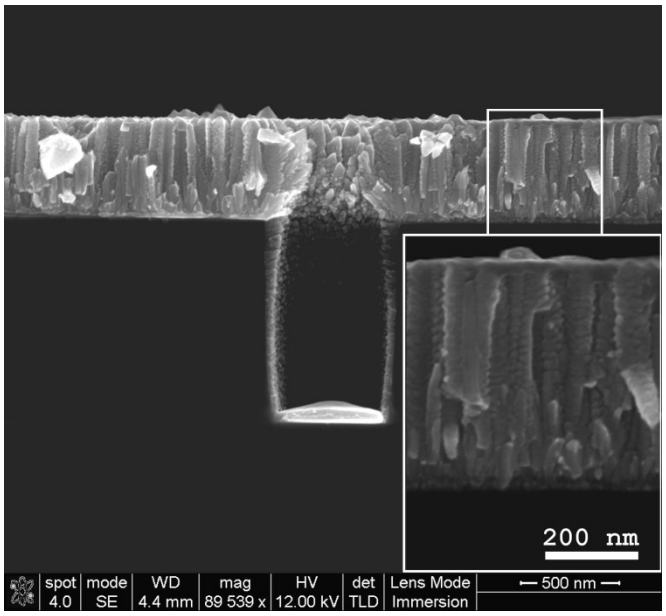

Figure 8d SEM cross section of Ni coated high aspect ratio vias deposited with 4000 W RF-Power at 6.4 Pa. The dense columnar structure with dendritic features can be seen. The insert shows the magnified coating structure.

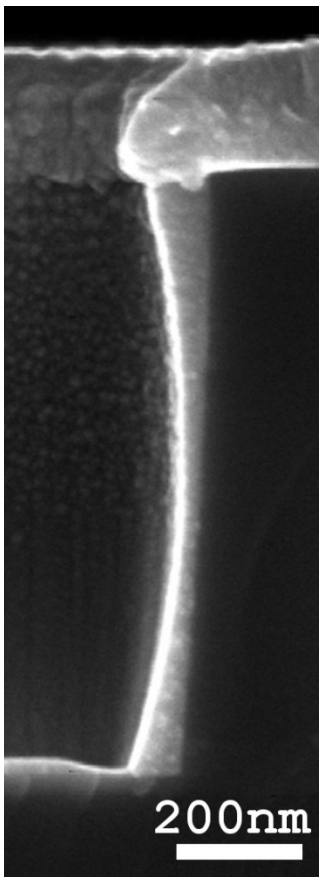

Figure 9a Close up of the corner of the via from figure 8b (deposition at 14 Pa) showing dense globular growth of the Ni coating. Sidewalls and bottom of the via are evenly coated indicating high metal ionisation and modest resputtering from bottom

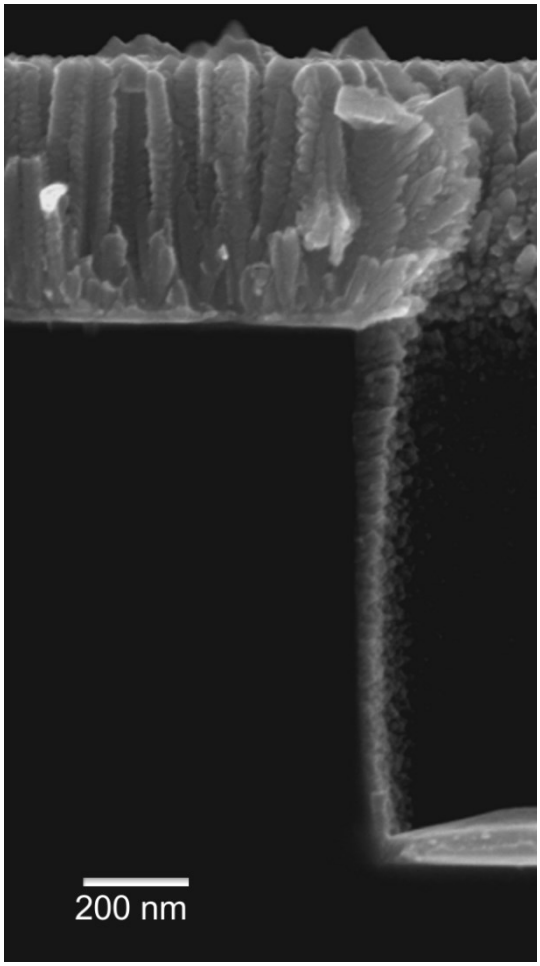

Figure 9b Close up of the corner of the via from figure 8d (6.4 Pa). Dendritic growth of the Ni coating can be seen along with the perpendicular growth on the sidewalls.

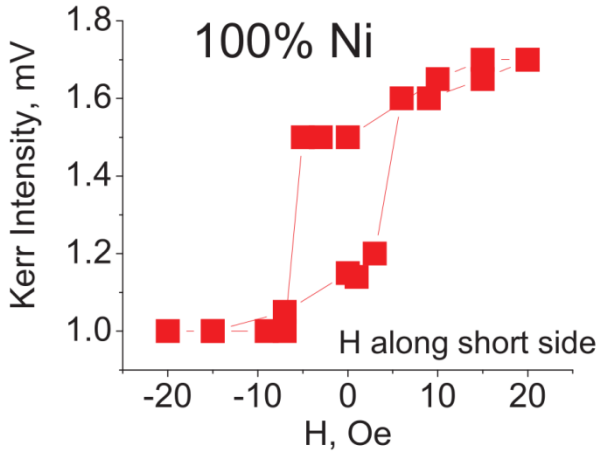

a.

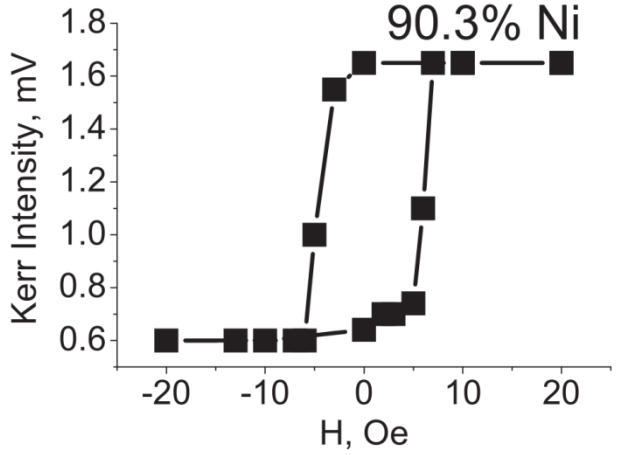

b.

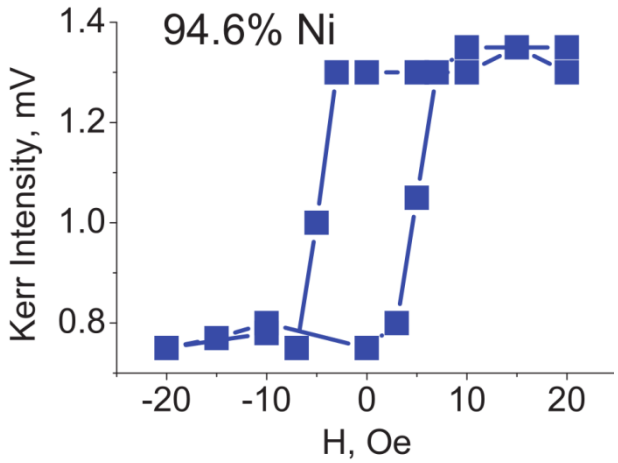

c

Figure 10a-c Comparision of MOKE results for Samples a,b and c. As can be seen b and c are similar while a has a slope in values above coecivity

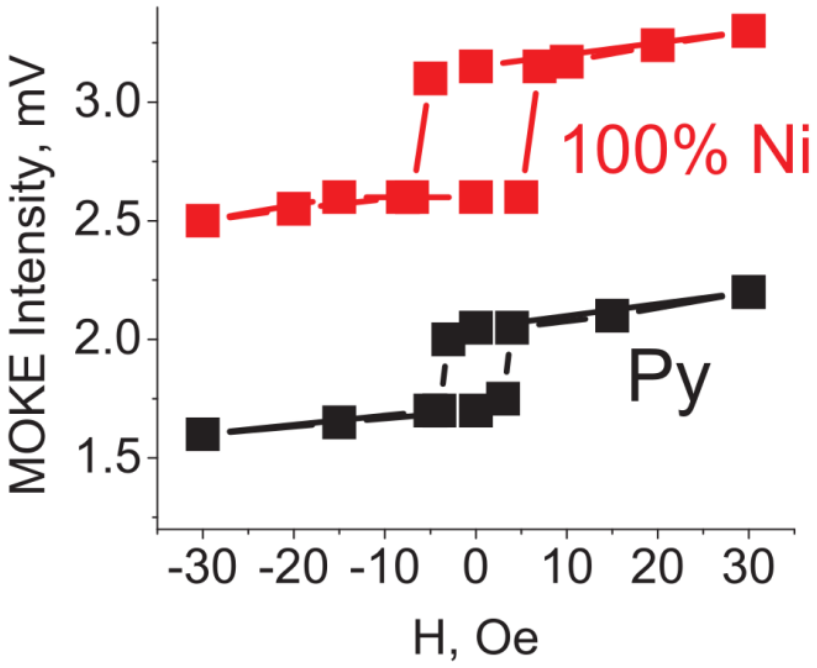

Figure 11 MOKE comparison of pure Ni coating with a standard reference sample of Py (80%Ni, 20%Fe).